

RESEARCH ARTICLE | JANUARY 02 2025

Filled colloidal gel rheology: Strengthening, stiffening, and tunability

Yujie Jiang  ; Yang Cui; Yankai Li; Zhiwei Liu  ; Christopher Ness  ; Ryohei Seto  



J. *Rheol.* 69, 35–44 (2025)

<https://doi.org/10.1122/8.0000878>



View
Online



Export
Citation

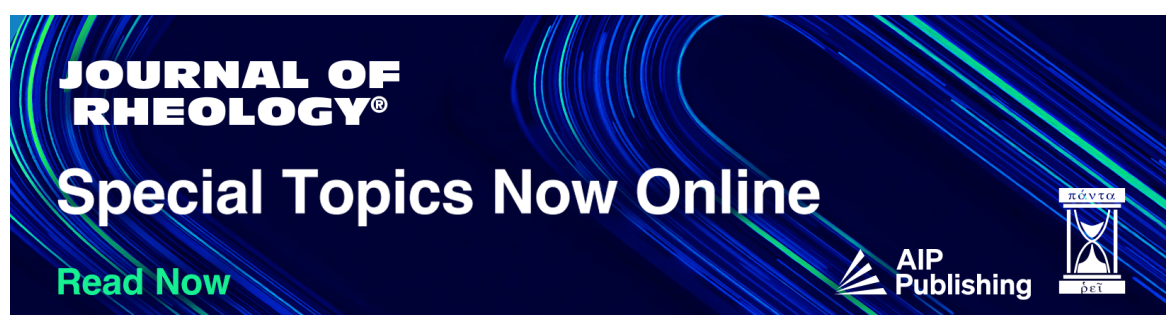
Related Content

KoopmanLab: Machine learning for solving complex physics equations

APL Mach. Learn. (September 2023)

Experimental realization of a quantum classification: Bell state measurement via machine learning

APL Mach. Learn. (September 2023)



The banner features the journal title "JOURNAL OF RHEOLOGY®" in white, bold, sans-serif font. Below it, the text "Special Topics Now Online" is displayed in a large, white, bold, sans-serif font. At the bottom left, a green button says "Read Now". On the right side, the AIP Publishing logo is shown, consisting of a stylized "A" icon followed by the text "AIP Publishing". The background of the banner is dark blue with abstract, glowing blue and green streaks resembling light trails or liquid flow.





Filled colloidal gel rheology: Strengthening, stiffening, and tunability

Yujie Jiang,^{1,2,a)} Yang Cui,^{1,3} Yankai Li,^{1,3} Zhiwei Liu,^{1,4} Christopher Ness,^{3,b)} and Ryohei Seto^{1,4,5,c)}

¹*Wenzhou Key Laboratory of Biomaterials and Engineering, Wenzhou Institute, University of Chinese Academy of Sciences, Wenzhou, Zhejiang 325000, China*

²*School of Mathematics and Physics, University of Science and Technology Beijing, Beijing 100083, China*

³*School of Engineering, The University of Edinburgh, King's Buildings, Edinburgh EH9 3FG, United Kingdom*

⁴*Oujiang Laboratory (Zhejiang Lab for Regenerative Medicine, Vision and Brain Health), Wenzhou, Zhejiang 325000, China*

⁵*Graduate School of Information Science, University of Hyogo, Kobe, Hyogo 650-0047, Japan*

(Received 12 May 2024; final revision received 10 November 2024; published 2 January 2025)

Abstract

Filler-induced strengthening is ubiquitous in materials science and is particularly well-established in polymeric nanocomposites. Despite having similar constituents, colloidal gels with solid filling exhibit distinct rheology, which is of practical interest to industry (e.g., lithium-ion batteries) yet remains poorly understood. We show, using experiments and simulations, that filling monotonically enhances the yield stress (i.e., strength) of colloidal gels while the elastic modulus (i.e., stiffness) first increases and then decreases. The latter softening effect results from a frustrated gel matrix at dense filling, evidenced by a growing interphase pressure. This structural frustration is, however, not detrimental to yielding resistance. Instead, fillers offer additional mechanical support to the gel backbone via percolating force chains, decreasing the yield strain at the same time. We develop a mechanistic picture of this phenomenology that leads us to a novel “filler-removal protocol,” making possible individual control over the strength and brittleness of a composite gel. © 2025 Published under an exclusive license by Society of Rheology. <https://doi.org/10.1122/8.0000878>

I. INTRODUCTION

Attractive colloids self-assemble into percolating, porous gel networks, leading to soft solids with finite yield stress [1–5]. These colloidal gels constitute an important material class in industries ranging from consumer products to coatings and biotechnology [6–8]. Hence, understanding and controlling their rheology is of broad fundamental interest and practical importance. The intrinsic dynamical arrest associated with colloidal gelation [9–13] naturally frustrates mechanical tunability, though several recent works seek to achieve this via nonequilibrium protocols comprising external flow [14], acoustic vibration [15], and active doping [16,17]. Nonetheless, the exploration of more efficient rheological control strategies is still in progress.

Solid filling is a widely used technique for reinforcement, such as in polymer nanocomposites [18], filled resins [19], and concretes [20]. The size disparity between the constituents (i.e., matrix $\sim \text{\AA}$ vs filler $\gtrsim \text{nm}$) generally enables these materials to be characterized by application of standard approaches in continuum mechanics [21,22]. In particle-filled colloidal gels, these lengthscales are comparable ($\sim \mu\text{m}$), and their interplay generates novelty not describable by conventional models. For example, adding non-Brownian grains to a colloidal gel leads

to a mechanorheological material in which external flow triggers a unique bistability [23]. Meanwhile, filling nontrivially distorts the gelation diagram boundaries [24], governed in part by competing lengthscales that emerge [25].

As the addition of fillers reduces the volume available for colloids, the simplest characterization of a filled gel is by its effective volume fraction ϕ_{eff} , subtracting the filler volume from the total as

$$\phi_{\text{eff}} \equiv \frac{V_{\text{gel}}}{V_{\text{total}} - V_{\text{filler}}} = \frac{\phi_g}{1 - \phi_f}, \quad (1)$$

where ϕ_g and ϕ_f refer to the absolute volume fractions of gel colloids and filler particles, respectively. Hence, a filled gel is more concentrated than an unfilled gel at the same ϕ_g . Filler-induced strengthening, reported in various colloidal gels [26,27], is qualitatively described in part by the increase in ϕ_{eff} , yet quantitatively this measure fails to capture the filled gel properties [25,28]. With increasing attention being paid to composite materials, as well as their utility in technological applications (e.g., lithium batteries [29]), solid filling is considered a promising approach to tuning gels efficiently [30,31]. A fundamental understanding of the basic physics governing filled-gel rheology is, therefore, crucial.

The parameter space of filled gel composites is huge, and industrial formulations vary from product to product [32,33]. In this work, we focus on a minimal model system: a strongly aggregating colloidal gel with embedded large, non-sticky fillers. In experiments, we observe an anomalous inconsistency between the ϕ_f dependence of the stiffness,

^{a)}Electronic mail: yjjiang@ustb.edu.cn

^{b)}Electronic mail: chris.ness@ed.ac.uk

^{c)}Author to whom correspondence should be addressed; electronic mail: seto@ucas.ac.cn

represented by the elastic (or storage) modulus G' , and the strength, represented by the yield stress σ_y . Simulations corroborate this finding, allowing us to unravel the different roles of filling in the above two cases. Incorporating a length-scale argument, our results lead to a mechanistic description that not only has important practical implications (e.g., in battery processing [34] and geophysical flow [35]), but also suggests a conceptual pathway to tunable soft composites.

II. METHODS

A. Experimental materials

Our experimental model system of filled gel contains two batches of silica particles dispersed in an aqueous solvent. The gel colloids are stöber silica of diameter $d_g \approx 482$ nm (from light scattering), functionalized with trimethylsilyl groups to render hydrophobicity [36]. The fillers are regular silica microspheres of diameter $d_f \approx 4 \mu\text{m}$ (from Blue Helix Ltd.), approximately eight times larger than the colloids. For confocal imaging, dyes are incorporated into the small colloids and the nearly refractive-index-matched solvent of ethanol, water, and glycerol (1:1:9 mass ratio). Confirmed by microscopy and rheology, the silica colloids strongly attract each other ($U_a \gg k_B T$) via hydrophobic interactions, while the fillers are nearly hard spheres with short-ranged electrostatic repulsion (Debye length $\kappa \approx 10$ nm). When mixed, the colloids aggregate into a porous gel network with fillers embedded inside, Fig. 1(a). The absence of colloidal “halo” precludes strong attractions between gel colloids and fillers, see Fig. S1 in the [supplementary material](#).

For filled colloidal gels, we fix the absolute volume fraction of gel colloids at $\phi_g = 0.1$, which gives a tenuous solid-like gel, and we vary the volume fraction ϕ_f of fillers.

B. Simulations

Using LAMMPS [37], our simulation system consists of attractive gel colloids with an average diameter d_g (bidisperse with 1:1.3 to prevent crystallization) and large fillers with diameter $d_f = 8d_g$ in a cubic box with Lees–Edwards periodic boundaries. Based on the pair types (g-g, g-f, and f-f), three interactions are considered. For simplicity, both

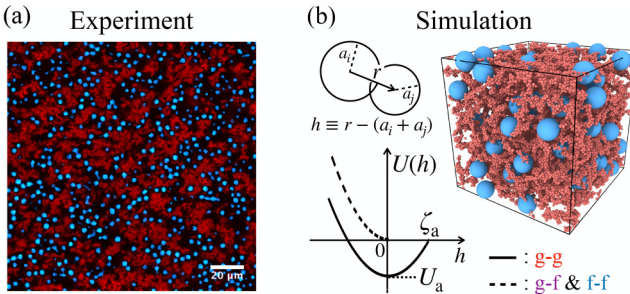


FIG. 1. (a) Colloidal gels with particle fillers in experiments (confocal slice). Red: gel colloids with $\phi_g = 0.1$; blue: solid fillers with $\phi_f = 0.2$. (b) 3D rendering of a simulation in similar conditions to (a). The interactions (potential curves) used in the simulations are sketched on the left. $h \equiv r - (a_i + a_j)$ refers to the surface distance between the i th particle with radius a_i and the j th particle with radius a_j . r refers to the center-to-center distance.

volume exclusion (among all particles) and g-g attraction (between gel colloids) are modeled using Hookean springs with a unified stiffness k , i.e., harmonic potentials as shown in Fig. 1(b). Attraction is set to be short-ranged ($\zeta_a = 0.01d_g$) and strong ($U_a \equiv k\zeta_a^2/2 = 20k_B T$) [38], giving the interaction stress scale $U_a d_g^{-3}$.

Analogous to experiments, we fix the gel volume fraction at $\phi_g = 0.1$ and vary that of fillers ϕ_f . To prevent finite size effects, all simulations contain at least $N_g = 40\,000$ gel colloids, i.e., the box size $L \gtrsim 60d_g$. Gelation begins from a random configuration and proceeds over $10^3 \tau_B$ under a Langevin thermostat until reaching a stable gel, where $\tau_B \equiv \pi\eta d_g^3/2k_B T$ is the Brownian time scale of gel colloids with solvent viscosity η . We then relax the gel by gradual quenching to $k_B T = 0$. Our primary focus in this study is the effect of fillers on the network morphology and the resulting mechanics. As we consider sufficiently strong colloidal bonding, dynamical effects (e.g., caging effects [39] and the glass transition [40]) contribute little to the rheology. Therefore, adapted from [41], our simulations measure the rheology at athermal conditions following a full quench.

Throughout this work, each simulation runs five times, with the presented data and error bars representing the average (or geometric mean) and standard deviation, respectively. We use OVITO [42] to render visualization.

C. Rheology

For both experiments and simulations, we measure the rheology once the gel is fully formed. Rheological measurements comprise small amplitude oscillatory shear (SAOS) and creep test, giving the elastic modulus G' and yield stress σ_y , respectively.

Before each experimental measurement, we perform a high-rate rejuvenation at $\dot{\gamma} = 1000 \text{ s}^{-1}$ for 1 min and a subsequent 30 min recovery at rest to prevent the phase separation as reported in [23]. Rheology is then measured on a stress-controlled, Anton Paar MCR 301 rheometer with a sandblasted cone-plate geometry (cone angle 1°; diameter 25 mm; truncation gap 48 μm). SAOS is carried out with strain amplitude $\gamma_0 = 0.1\%$ and a low frequency $\omega = 1 \text{ rad s}^{-1}$, with 30 s equilibration and subsequent 60 s measurement. These guarantee reproducible measurements in the linear regime (see Fig. S2 in the [supplementary material](#)). For creep tests [43], we start from a small stress $\sigma = 0.1 \text{ Pa}$ and increase it in a stepwise manner until steady flow ($\dot{\gamma} \approx \text{constant}$ and $\dot{\gamma} > 0$) occurs. Imposing a constant stress σ , we measure the strain evolution for at least 5 min, which is sufficiently long for the shear rate $\dot{\gamma}$ to be either vanishing (below yielding) or finite (beyond yielding).

In simulations, SAOS is carried out at the same amplitude ($\gamma_0 = 0.1\%$) and a low frequency ω (see Fig. S3 in the [supplementary material](#)). Compared with the damping time $t_d \equiv m_g/3\pi\eta d_g$ (where m_g refers to the particle mass), the oscillation is slow enough ($\omega t_d \approx 0.01$) to eliminate inertial effects. Oscillation proceeds for five full cycles, with the first two cycles for equilibrating and the last three cycles for averaging measurement. With the time series of shear stress $\sigma(t)$ and sinusoidal shear strain $\gamma = \gamma_0 \sin(\omega t)$, we use Fourier

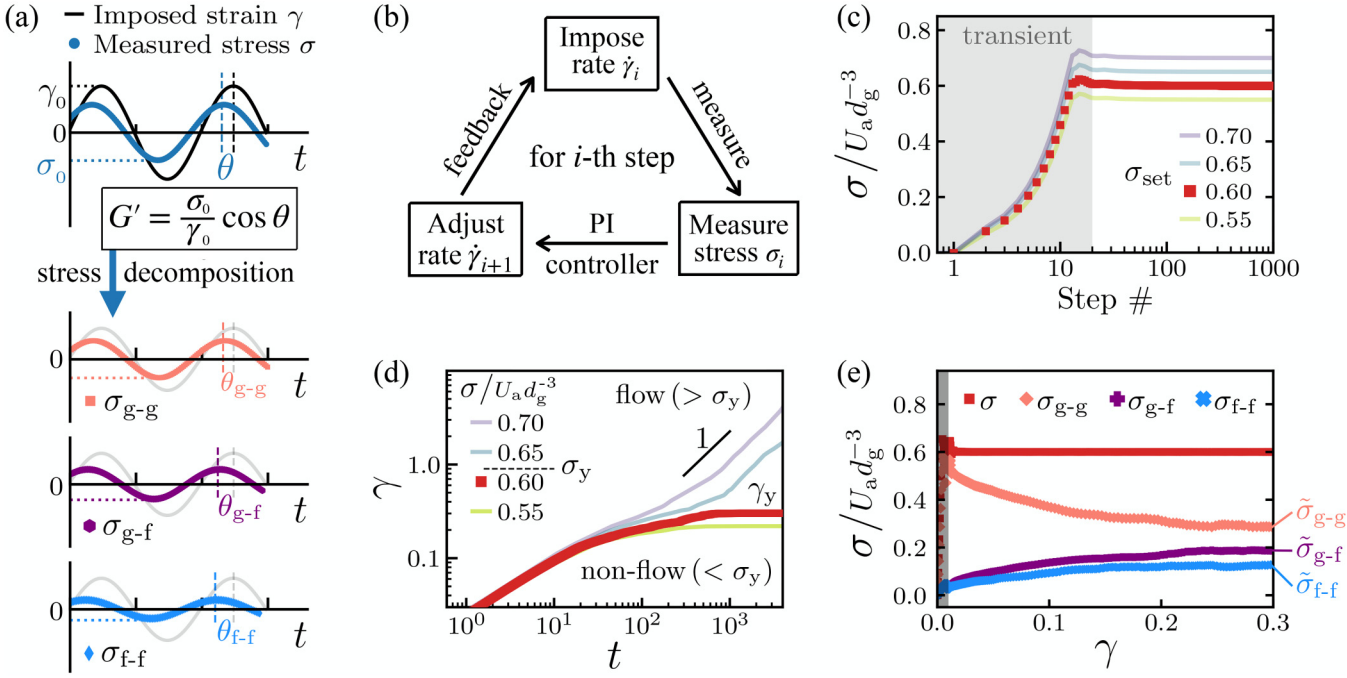


FIG. 2. Rheology measurements in simulations. (a) Stress signals in oscillatory rheology (SAOS) and modulus decomposition. (b) Schematic feedback loop in stress-controlled simulations. (c)–(e) Creep test results of a filled gel at $\phi_f = 0.4$. (c) Under a series of setpoints σ_{set} , the measured stress σ equilibrates at σ_{set} within 20 simulation steps (transient region). (d) The strain γ evolves over time under creep tests, either reaching a finite value (nonflow, $\sigma < \sigma_y$) or linearly growing (flow, $\sigma > \sigma_y$). (e) For the data just below the yield stress [$\sigma/U_a d_g^{-3} = 0.60$, with filled square symbols (red) in (c) and (d)], the stress σ is further decomposed by pair species [see Eq. (3)], and their evolutions over strain γ . The stable values ($\tilde{\sigma}_{g-g}$, $\tilde{\sigma}_{g-f}$, and $\tilde{\sigma}_{f-f}$) refer to the yield strength contributions.

Transform to extract the stress amplitude σ_0 and phase difference θ , giving the elastic modulus $G' = (\sigma_0/\gamma_0)\cos\theta$ as shown in Fig. 2(a).

Rheological simulations on LAMMPS are intrinsically rate-controlled. To achieve creep tests, we implement a feedback loop [44] internally to maintain a constant shear stress σ by adjusting the shear rate $\dot{\gamma}$ at every single step, Fig. 2(b). Given a setpoint σ_{set} , we measure the shear stress $\sigma(t)$ and then impose a corresponding shear rate $\dot{\gamma}(t)$ based on the distance to the setpoint, i.e., the error value $e(t) \equiv \sigma(t) - \sigma_{\text{set}}$. Specifically, a proportional-integral (PI) controller is applied as follows:

$$\dot{\gamma}(t) = K_p e(t) + K_i \int_0^t e(t) dt, \quad (2)$$

where K_p and K_i are two control parameters. With appropriate parameter tuning, such a method can stabilize the stress σ around the setpoint (with $\lesssim 1\%$ error) in 20 simulation steps, such as Fig. 2(c). By imposing a series of shear stresses, we examine the evolution of strain $\gamma(t)$ to determine the nonflow ($\dot{\gamma} \approx 0$) and flow ($\dot{\gamma} \approx \text{constant}$ and $\dot{\gamma} > 0$) states, as well as the yield stress σ_y and yield strain γ_y as shown in Fig. 2(d).

1. Stress decomposition

In simulations, we keep the shear rates ($\gamma_0\omega$ in oscillatory rheology and $\dot{\gamma}$ in creep test) sufficiently small to eliminate inertial effects. This enables us to ignore the kinetic contribution ($\propto mv^2$) and bulk viscous stress ($\propto \eta\dot{\gamma}$) in the shear stress σ . To gain mechanistic insight, we decompose σ into contributions from each of three interacting pairs,

$$\sigma = \sigma_{g-g} + \sigma_{g-f} + \sigma_{f-f}, \quad (3)$$

then obtain the corresponding moduli G'_{g-g} , G'_{g-f} , and G'_{f-f} by Fourier transformation of the respective signals, Fig. 2(a). The linearity ensures $G' = G'_{g-g} + G'_{g-f} + G'_{f-f}$ (see demonstration in the [supplementary material](#)).

Similarly, the yield stress σ_y measured from the creep test can be decomposed as well. For the stress just below yielding ($\sigma \rightarrow \sigma_y^-$), we apply stress decomposition Eq. (3) to show the evolution of each component, Fig. 2(e). The stress value in the equilibrium state ($\gamma \rightarrow \gamma_y$) then represents the contribution of each interaction type to the overall yield strength, denoted by $\tilde{\sigma}_{g-g}$, $\tilde{\sigma}_{g-f}$, and $\tilde{\sigma}_{f-f}$.

III. RESULTS

A. Unfilled gel rheology

We first investigate the rheology of unfilled colloidal gels, i.e., $\phi_f = 0$. In experiments, both the elastic modulus G' (from SAOS) and the yield stress σ_y (from creep test) monotonically increase with the volume fraction of gel colloids ϕ_g , Fig. 3(a). Power-law fittings give $G' = 2.27 \times 10^6 \phi_g^{4.22} \text{ Pa}$ (blue solid line) for elastic modulus and $\sigma_y = 1.7 \times 10^3 \phi_g^{3.27} \text{ Pa}$ (red dashed line) for yield stress. The exponents are roughly consistent with those in the literature (such as the “strong-link gel” in [45]), indicating strong attractions between colloids.

Similar to experimental results, G' and σ_y in simulations also increase with ϕ_g in power-law manners, Fig. 3(b). Fittings give $G'/U_a d_g^{-3} = 29.8 \phi_g^{2.31}$ and $\sigma_y/U_a d_g^{-3} = 19.1 \phi_g^{1.73}$, respectively. Though still consistent with literature values

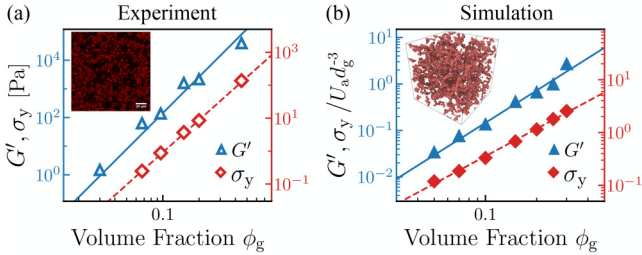


FIG. 3. Unfilled gel rheology in experiments (a) and simulations (b). Elastic modulus G' (blue triangle) and yield stress σ_y (red diamond) vary as functions of gel volume fraction ϕ_g . Solid and dashed lines are power-law fittings. For experiments, $G' = 2.27 \times 10^6 \phi_g^{4.22}$ Pa and $\sigma_y = 1.7 \times 10^3 \phi_g^{3.27}$ Pa. For simulations, $G'/U_a d_g^{-3} = 29.8 \phi_g^{2.31}$ and $\sigma_y/U_a d_g^{-3} = 19.1 \phi_g^{1.73}$.

[46–49], both the exponents are lower than those of experimental gels. This quantitative discrepancy may result from the simplified interactions used in our simulations, which do not consider more complex and realistic effects such as hydrophobicity [50], frictions [51], and adhesions [40], among others. However, such a minimal model can help us efficiently uncover the key physics of composite gels. The qualitative agreement also supports our methodology.

B. Rheological inconsistency in filled gels

With the volume fraction of gel colloids $\phi_g = 0.1$ fixed, we investigate how the addition of fillers affects the filled gel rheology. According to Eq. (1), fillers effectively concentrate the gel and, in principle, are expected to increase both G' and σ_y as predicted by the power laws in Fig. 3. As shown in Fig. 4, the yield stress σ_y (red squares) indeed increases monotonically with the filler volume fraction ϕ_f . The elastic modulus G' , on the contrary, exhibits a peak at $\phi_f^c \approx 0.3$ and then decreases, i.e., softening. Such a drop in modulus with dense filling conflicts with the expectation from increasing ϕ_{eff} (solid black lines) and deviates markedly from the trend of increasing yield strength. Despite the quantitative differences, this inconsistency is observed in both experiments and simulations, Fig. 4.

C. Nonmonotonic elastic modulus

To uncover the origin of softening, we apply the stress/modulus decomposition [Fig. 2(a)] to the filled gels in simulations. In the low-filling regime ($\phi_f \lesssim \phi_f^c$), the elastic response is dominated by that of the gel matrix G'_{g-g} , Fig. 5(a). Here, fillers are mostly isolated, or *loosely confined*, within the gel matrix as shown in Fig. 5(c) (left). The occasional gel-filler and filler-filler contacts are unsustainable and thus respond viscously, leading to vanishing G'_{g-f} and G'_{f-f} in Fig. 5(a).

Extending the power law of unfilled gels to filled gels, we find that the elastic modulus predicted using ϕ_{eff} in place of ϕ_g [solid black line in Fig. 5(a)] appears to capture well the measured G' below ϕ_f^c . That is, consistent with accelerated gelation [25], fillers concentrate the gel matrix in a manner effectively described by ϕ_{eff} . While such $G'-\phi_{\text{eff}}$ scaling is expected locally, this is not trivial on a global level since loosely confined fillers generate cavities in the gel network. Presumably, both the stress and strain are associated with

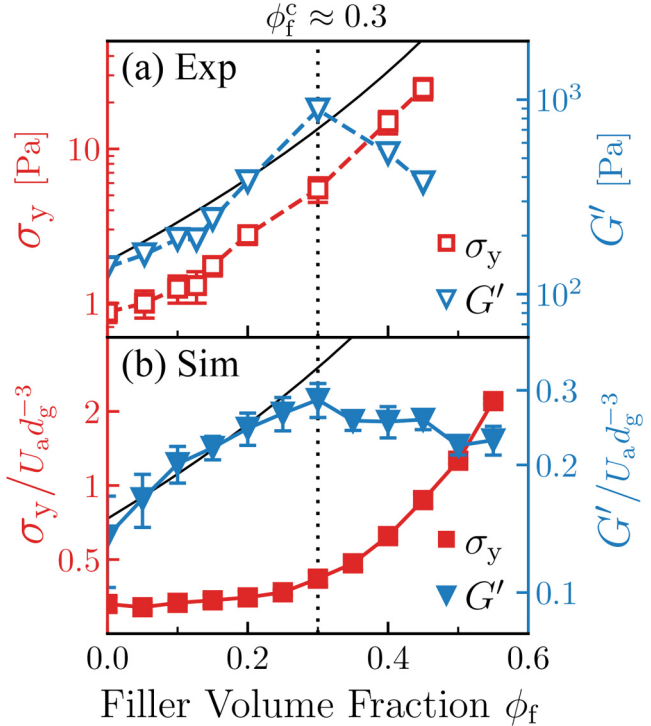


FIG. 4. Rheological inconsistency in granular-filled colloidal gels. (a) Experimental (Exp) data of yield stress σ_y and elastic modulus G' are plotted as functions of filler volume fraction ϕ_f . The solid black line refers to the ϕ_{eff} -predicted elastic moduli, giving $G' = 2.27 \times 10^6 \phi_{\text{eff}}^{4.22}$ Pa. (b) Simulation (Sim) data of σ_y and G' in semilogarithmic plots. The solid black line shows $G'/U_a d_g^{-3} = 29.8 \phi_{\text{eff}}^{2.31}$.

their local counterparts by a factor of $\sim(1 - \phi_f)^{-1}$ (cf. [52]) so that they cancel out in G' .

As filling increases ($\phi_f \gtrsim \phi_f^c$), fillers start to *frustrate* and thereby weaken the gel skeleton via direct contacts, Fig. 5(c) (right). This is evidenced by the decreased gel modulus G'_{g-g} , which decays faster than the overall elastic modulus G' . While the gel-matrix contribution still dominates, the filler-induced moduli G'_{g-f} and G'_{f-f} emerge above ϕ_f^c and increase with filling, Fig. 5(a). This implies that the fillers are persistently trapped within the gel skeleton via mechanical contacts, which enable them to participate directly in structural percolation and stress transmission.

In contrast to the sparsely filled gels, fillers ($\phi_f > 0.3$) participating in the load-bearing network serve as junctions and thus induce heterogeneous stress transmission [53]. In addition, the gel-filler and filler-filler pairs cannot support tensile loads, unlike the gel-gel matrix, where both tension and compression generate elastic forces. Together, these factors result in less efficient stress transmission and, therefore, a reduction in elastic modulus G' .

Moreover, the mechanical frustration from gel-filler contacts above ϕ_f^c plays a role. We characterize this frustration using the interphase particle pressure

$$\Pi_{g-f} \equiv -\frac{1}{3} \text{tr}(\Sigma_{g-f}), \quad (4)$$

where Σ_{g-f} denotes the gel-filler stress tensor measured at rest. At low filling $\phi_f \lesssim \phi_f^c$, the vanishing interphase pressure

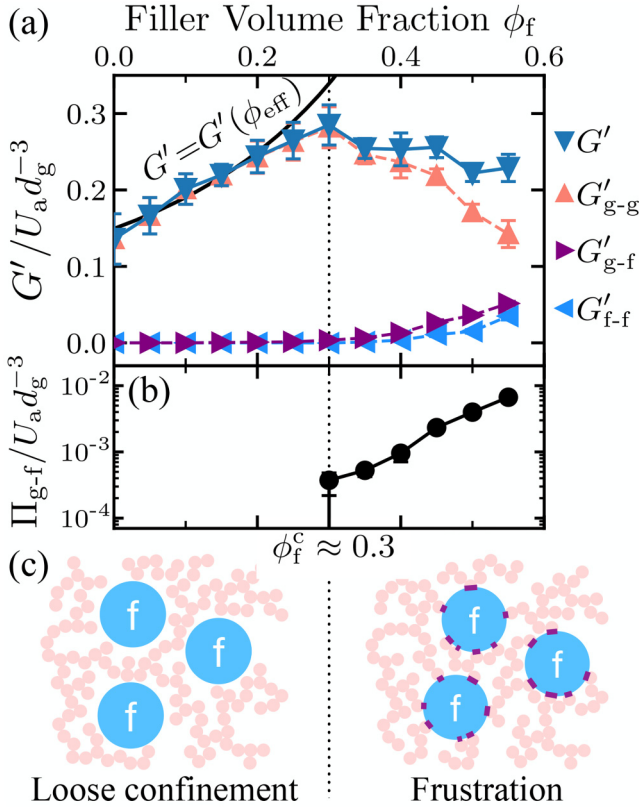


FIG. 5. Decomposition of elastic modulus G' . (a) Decomposed elastic moduli as functions of filler volume fraction ϕ_f . Solid line: $G'/U_a d_g^{-3} = 29.8 \phi_{\text{eff}}^{0.31}$ with ϕ_{eff} defined in Eq. (1). (b) Interphase pressure Π_{g-f} . Here, we use the geometric mean for Π_{g-f} , which is nonzero for $\phi_f \geq \phi_f^c$. (c) Schematic gel matrices at low $\phi_f < \phi_f^c$ (left: loosely confined) and high $\phi_f \geq \phi_f^c$ (right: mechanically frustrated). Interphase contacts are highlighted.

$\Pi_{g-f} = 0$ [Fig. 5(b)] is consistent with the absence of G'_{g-f} in Fig. 5(a), again confirming loosely confined fillers.

At high filling $\phi_f \gtrsim \phi_f^c$ and with sufficient relaxation prior to measurement, Π_{g-f} , or equivalently the frustration on the gel, cannot be fully relaxed due to the limited free space. Instead, it becomes nonzero beyond $\phi_f^c \approx 0.3$ and increases with ϕ_f , Fig. 5(b). This coincides with the observed finite elastic responses from solid fillers (G'_{g-f} and G'_{f-f}), indicating a change in the stress transmission mode. Such filler-induced prestress [54] also suggests another possible origin of softening in G' .

1. Lengthscale scenario

A simple lengthscale argument seems to capture the deviation in G' from the ϕ_{eff} prediction reported here. For colloidal gels, a characteristic lengthscale ξ can be estimated from the primary peak of static structure factor $S(q)$, Fig. 6(a) and Fig. S4 in the supplementary material. As ξ decreases with ϕ_g according to a power-law as $\xi/d_g = 1.44\phi_g^{-0.88}$ (solid line), we assume such a scaling holds in filled gels by replacing ϕ_g with ϕ_{eff} . Another relevant lengthscale is the average spacing between fillers δ , which has been verified as important in various gel composites [26,55]. Through Voronoi analysis, we show how δ , almost independent on ϕ_g , decreases with ϕ_f , Fig. 6(b).

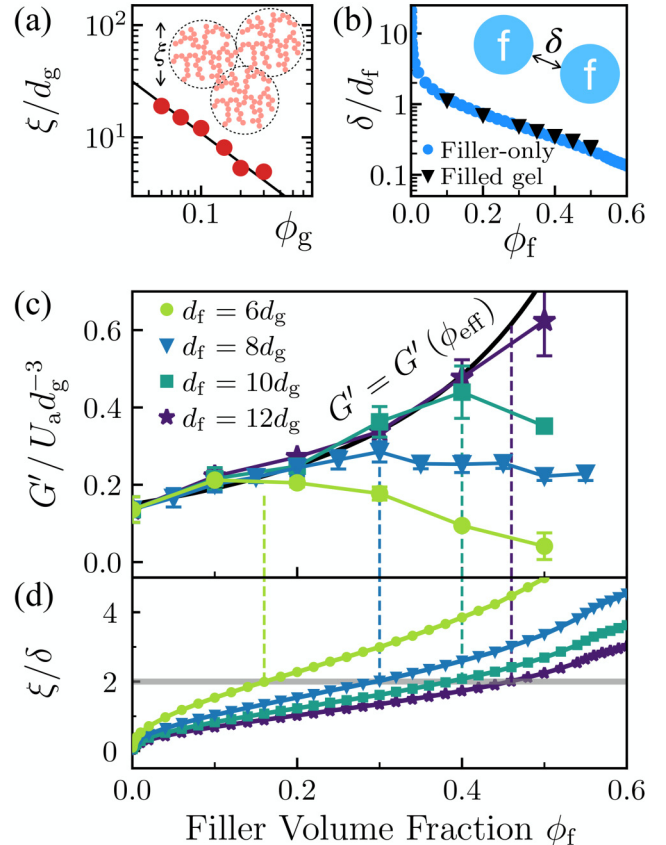


FIG. 6. Lengthscale scenario. (a) Characteristic gel length ξ varies with volume fraction ϕ_g in colloidal gels. Extracted from structure factors shown in Fig. S4 in the supplementary material. The solid line refers to power-law fitting: $\xi/d_g = 1.44\phi_g^{-0.88}$. (b) Filler spacing δ as a function of filler volume fraction ϕ_f in both filler-only systems ($\phi_g = 0$) and filled gels (various ϕ_g). The average spacing δ is measured from the equivalent sphere diameters of Voronoi cells. (c) Elastic modulus G' as a function of filler volume fraction ϕ_f at different filler sizes d_f . (d) Lengthscale ratio ξ/δ . The horizontal gray solid line refers to the critical value $\xi/\delta = 2$. The vertical dashed lines refer to the crossover points.

When the ratio of the two lengthscales ξ/δ is small, aggregated clusters can be naturally accommodated between fillers without being disturbed (i.e., loose confinement), forming a colloidal gel network well characterized by ϕ_{eff} . As the ratio increases, the reduction in free space leads to inevitable frustration on the gel matrix. A critical value $\xi/\delta = 2$ [dashed gray line in Fig. 6(d)], which captures the deviation of gelation time in [25], also coincides with the transition of G' away from the unfilled prediction in Fig. 6(c) (blue triangle) at $\phi_f^c \approx 0.3$. Importantly, this lengthscale argument appears to hold for various filler sizes d_f as shown in Figs. 6(c) and 6(d), suggesting a general physics of lengthscale interplay.

While the gel volume fraction $\phi_g = 0.1$ is fixed in this work, we expect the critical lengthscale ratio $\xi/\delta = 2$ to still apply within a range of ϕ_g by simply changing ξ . Yet a colloidal gel network is typically porous and of multiple scales. For very low ϕ_g where the gel clusters are highly porous, the fillers may be accommodated within the clusters, invalidating the comparison between cluster size ($\sim \xi$) and filler spacing ($\sim \delta$). For higher ϕ_g , the gelation proceeds in a manner of viscoelastic phase separation [56], where a percolated network is formed before coarsening and clustering. In such

case, disturbance on the final gel structure is limited. Hence, a generic framework of lengthscale interplay may require the incorporation of multiple physical quantities.

D. Yielding resistance

Although mechanical frustration caused by dense filling reduces the stiffness, it does not affect the yielding resistance; the yield stress σ_y monotonically increases with ϕ_f , Fig. 4. Creep test and stress decomposition illustrate the microscopic origin. For filled gels with low ϕ_f , the stress is mostly undertaken by the gel matrix [Fig. 7(a), upper], i.e., $\tilde{\sigma}_{g-g} \approx \sigma_y$ as shown in Fig. 7(d). This supports our argument that fillers are loosely confined and, therefore, their stress can be relaxed under load prior to yielding. Below ϕ_f^c , the strengthening in the yield stress σ_y is subtle.

As ϕ_f increases, the other two components ($\tilde{\sigma}_{g-f}$ and $\tilde{\sigma}_{f-f}$) grow and even exceed $\tilde{\sigma}_{g-g}$ beyond $\phi_f = 0.5$, Fig. 7(d). This differs from G' in Fig. 5(a), where G'_{g-f} and G'_{f-f} are always below G'_{g-g} . In a highly filled gel, such as $\phi_f = 0.4$ in Fig. 7(a) (lower), the fillers develop into percolating force chains along the compressive direction under shear. Moreover, the fillers, initially unaggregated, are pushed together under creeping shear and form clusters of fillers which persist under stress, such as Fig. 7(c). Under confinement of gel matrix, the largest cluster size L_f^{lc} increases with ϕ_f and percolate beyond $\phi_f = 0.35$ as shown in Fig. 7(b), greatly resisting yielding as a result. This is reminiscent of the percolation threshold in polymer nanocomposites [57], both leading to substantial strengthening. Further decomposing the gel response $\tilde{\sigma}_{g-g}$ into tensile and compressive components, we find that the ratio of compressive loads increases with ϕ_f [inset of Fig. 7(d)].

Surprisingly, in contrast to the filling-dependent G'_{g-g} shown in Fig. 5(a), the yield stress contribution $\tilde{\sigma}_{g-g}$ from the gel matrix remains almost independent of ϕ_f , Fig. 7(d). In other words, solid filling either enhances (loose confinement) or weakens (mechanical frustration) the stiffness G'_{g-g} of gel matrix depending on ϕ_f , but seemingly plays little role in the yielding resistance $\tilde{\sigma}_{g-g}$. This distinction is associated with the physical difference between the two quantities. The elastic modulus G' represents the stiffness of a material (i.e., how difficult to deform) and is typically measured at a small strain amplitude ($\gamma_0 = 0.1\%$ in this work). In contrast, yield stress σ_y , or strength, refers to the maximum load that a material can bear prior to failure, which usually occurs far beyond the linear regime ($\gamma_y \gtrsim 10\%$ in this work). This difference also determines whether the fillers percolate (yielding), such as Fig. 7(c), or not (SAOS). We conclude, therefore, that the monotonic strengthening in σ_y stems from the additional mechanical support offered by solid fillers, which may form percolating clusters when resist yielding.

E. Filler removal and tunability

The transition in yielding mechanism also manifests in the yield strain γ_y . Though quantitatively different [58], both experiments and simulations confirm that solid filling leads to a reduction in γ_y , Fig. 7(e). This embrittlement indicates more possibilities in tunable gel rheology. To further extend such tunability, as well as to better illustrate the role of solid filling, here we develop a *filler-removal protocol*. This protocol is inspired by the template-removal technique [59] in mesoporous materials. Specifically, we remove fillers following gelation and perform relaxation and rheological measurements afterward. The proportion α

07
JULY 2025
8015129

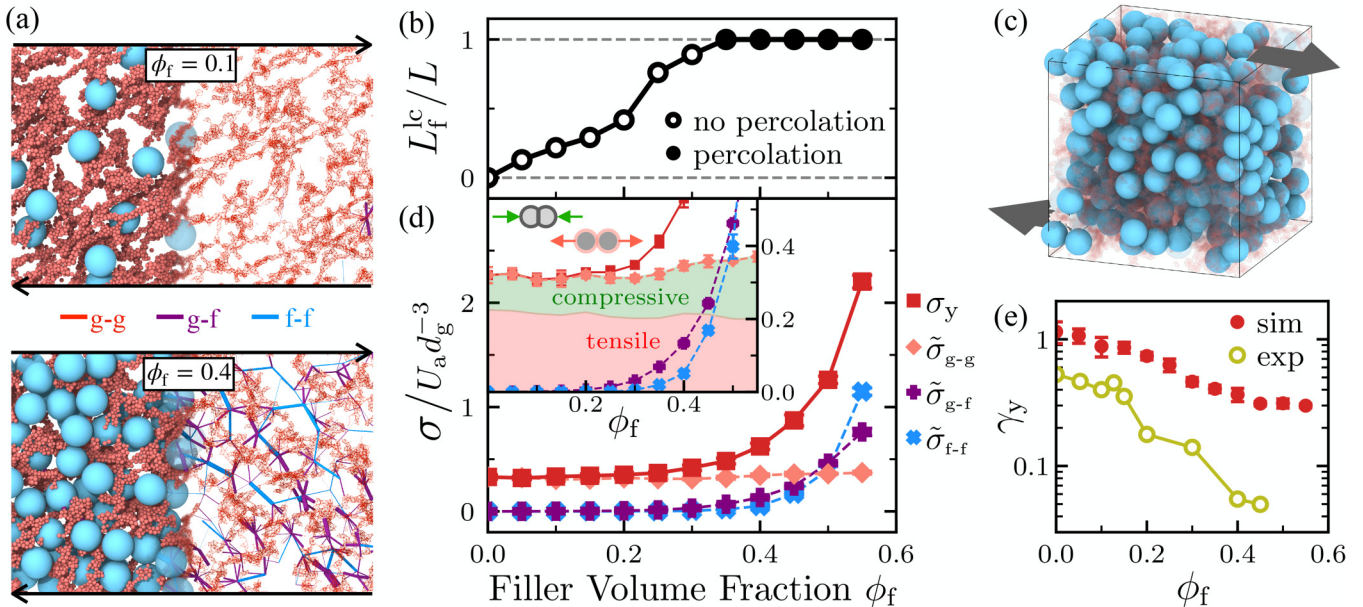


FIG. 7. Yielding resistance. (a) Interacting pairs of a dilutely filled gel (upper, $\phi_f = 0.1$) and a densely filled gel (lower, $\phi_f = 0.4$) prior to yielding ($\gamma \rightarrow \gamma_y$). Pair types are represented by different colors of bonds, whose width is proportional to the force magnitude. Slices with a thickness of $10d_g$ in the flow-gradient plane are shown. See full movies Videos S1 and S2 in the [supplementary material](#). (b) Size of the largest filler cluster L_f^{lc} , normalized by the box size L , under creep test ($\gamma \rightarrow \gamma_y$). Filled symbols represent percolated clusters. (c) An example of percolating filler cluster at $\phi_f = 0.4$. (d) Yield stress σ_y and contributions from each interacting pair type ($\tilde{\sigma}_{g-g}$, $\tilde{\sigma}_{g-f}$, and $\tilde{\sigma}_{f-f}$) as functions of filler volume fraction ϕ_f . Inset shows further decomposition of $\tilde{\sigma}_{g-g}$ into compressive and tensile loads. (e) Yield strains γ_y (determined by creep tests) from simulations (sim) and experiments (exp) as functions of filler volume fraction ϕ_f .

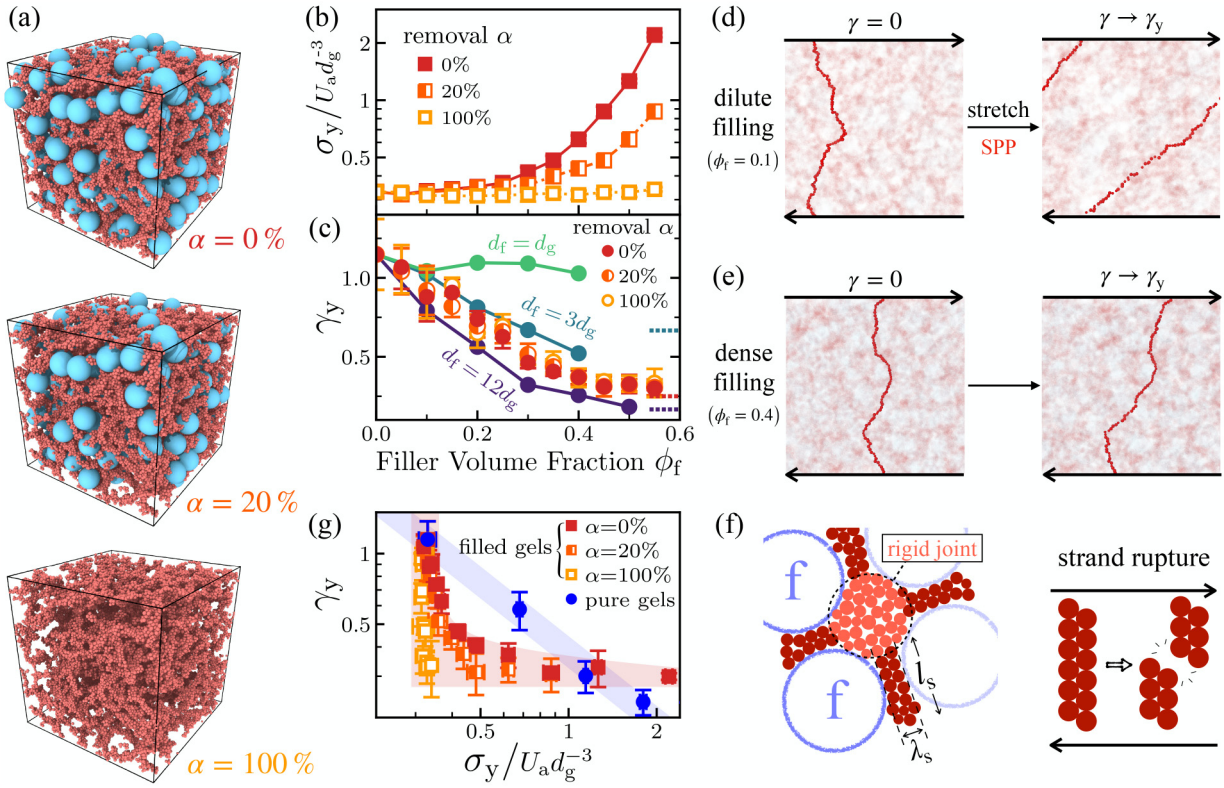


FIG. 8. Filler-removal protocol. (a) Filler-removal sketch with varying removal fraction α . (b) Yield stress σ_y as a function of filler volume fraction ϕ_f and removal fraction α . (c) Yield strain γ_y as a function of filler volume fraction ϕ_f , removal fraction α , and filler size d_f . Dashed lines on the right-hand side refer to the predicted $\gamma_y \sim \lambda_s/l_s$, see (f). (d) and (e) Stretched SPP (highlighted in red) under creeping of dilutely filled gel (d, $\phi_f = 0.1$) and densely filled gel (e, $\phi_f = 0.4$). See full structural evolutions Videos S3 and S4 in the [supplementary material](#). (f) Schematic strand rupture in densely filled gels upon yielding. (g) $\sigma_y - \gamma_y$ diagram of colloidal gels (blue solid circles) and filled gels ($d_f = 8d_g$) upon filler removal at different α .

JANUARY 2025 VOL 151 #1

of fillers to remove (randomly selected) then becomes a tuning parameter, Fig. 8(a).

While the yield strength monotonically increases with ϕ_f , removing all fillers ($\alpha = 100\%$) always reduces the yield stress σ_y to that of an unfilled gel, Fig. 8(b). This is consistent with the insignificant ϕ_f dependence of the stress contribution $\tilde{\sigma}_{g-g}$ from gel matrix, Fig. 7(b). In addition, a gel with partially removed fillers ($\alpha = 20\%$) exhibits an intermediate yield stress between those of a full composite ($\alpha = 0\%$) and a filler-removed matrix ($\alpha = 100\%$), Fig. 8(b). Regardless of the initial ϕ_f , the yield strength σ_y seems to be mainly determined by the remaining filler volume fraction $\phi_f(1 - \alpha)$, as shown in Fig. S5 in the [supplemental material](#). These results, as well as the lower G' upon filler removal (see Fig. S6 in the [supplemental material](#)), further elucidate the role of solid fillers in mechanical reinforcement.

Interestingly, the filler-removal operation appears to have little effect on the yield strain γ_y , Fig. 8(c). This implies the structural origin of filler-induced embrittlement. Though increasing the concentration typically reduces the yield strain in colloidal gels [45], the reduction in γ_y may not be simply attributed to the increasing ϕ_{eff} . With the same composition, the yield strain γ_y varies as a function of the filler size d_f . Larger fillers ($d_f = 12d_g$) give rise to lower γ_y ; comparable sizes ($d_f = d_g$) barely change γ_y , Fig. 8(c). These results suggest another size-dependent physics, which is not accounted for ϕ_{eff} in Eq. (1).

Dilute gels of strongly aggregating colloids consist of ramified clusters [60], in which thin strands are packed in a

fractal manner (see Fig. S4 in the [supplemental material](#)). With strong attractions, these strands hardly deform on their own [61], but their joints, instead, are relatively flexible to allow cluster rotations. Hence, the gel network evolves into a highly stretched state under shear [41], and the yielding point correlates with the fracture of the most-stretched strand, Fig. 8(d) and Video S3 in the [supplementary material](#). While network morphology is determinative to gel rheology [62], a quantitative analysis based on the shortest percolation path (SPP) [63] agrees with our measurement on γ_y for dilute gels (see Fig. S7 in the [supplemental material](#)).

Filling at high ϕ_f solidifies the joint-strand connections *via* squeezing. The gel is squeezed to fit in between compactly packed fillers, and the colloidal lumps (joints) only stay at the filling interstice, Fig. 8(f). If assuming fully constrained joints at the dense limit, yielding occurs with the rupture, rather than stretch [see Fig. 8(f) and Video S4 in the [supplemental material](#)], of the strands. The yield strain γ_y may be alternatively estimated by the aspect ratio of strands. While the strand length l_s is comparable to the filler size d_f as sketched in Fig. 8(f) (left), the width $\lambda_s \approx 2d_g$ can be approached by considering a strand of tetrahedrons (the minimal rigid element [64]). Thus, we can estimate the yield strain as $\gamma_y \sim \lambda_s/l_s$, which is d_f dependent.

For large d_f , the above estimate is in quantitative agreement with the simulations, Fig. 8(c) (dashed lines). Small fillers, nevertheless, behave more like a continuous fluid phase without modifying the final gel structure (see gel-gel

structure factor, Fig. S8 in the [supplementary material](#)) and thereby have less impact on γ_y . While the two yielding scenarios we proposed [Figs. 8(d)–8(f)] exhibit semiquantitative agreement with simulational measurements, experimental verifications are, unfortunately, unpractical due to the limited view and time resolution in microscopy.

The disparate dependence of yield stress and strain on filler removal allows for additional tunability. For colloidal gels, changing volume fraction merely enables limited exploration on the σ_y - γ_y diagram, Fig. 8(g) (blue solid circles). With the filler-removal protocol applied, the yield strength σ_y varies with both the filler volume fraction ϕ_f and the removal fraction α , while the yield strain γ_y is a function of ϕ_f only. This suggests a novel way to tune gel rheology. By replotted the data of Figs. 8(b) and 8(c) ($d_f = 8d_g$) in the same diagram, we find that filling techniques enable continuous exploration to a more brittle state (low σ_y and low γ_y), Fig. 8(g) (red squares), which is not naturally accessible by unfilled gels. That is, the filler-removal protocol enables individual control over strength and brittleness.

There are several candidate experimental protocols in which this computational proof-of-concept could be realized. One is to adapt current template-removal techniques, which utilize microwave [59], ultraviolet light [65], chemical reflux [66], etc. Using fillers of thermo-sensitive materials (e.g., pNIPAAm [67] and gelatin [68]), filler-removal protocol may also be achieved via temperature control. Alternatively, bubbles- or droplets-embedded gel composites [69–72] exhibit potential of practical filler removal as well. While these routes highly enrich the control diagram, tunability using other quantities, such as gel volume fraction ϕ_g [45], filler size d_f [Figs. 6(c) and 8(c)], and interparticle friction [73], presents a vast parameter space of rheological control by formulation that can be made rational by the mechanistic insight provided here.

IV. CONCLUSIONS

Altogether we probe the impact of solid filling on colloidal gel rheology, focusing on the case of large, nonsticky fillers embedded in a matrix of a dilute, yet strong ($U_a \gg k_B T$), colloidal gel. With more fillers added to the gel, the inconsistency between yield strength ($\sim \sigma_y$) and stiffness ($\sim G'$) indicates different roles of solid filling. Fillers can additionally support the gel matrix to resist further yielding under sustained load and large strain, whereas beyond $\phi_f^c \approx 0.3$ the structural frustration on the gel backbone dominates and leads to softening under small amplitude oscillatory shear. This structural impact also leads to a reduction in yield strain γ_y . Exploiting the novel filler-removal protocol described here, one may individually control the strength and brittleness to achieve a new practical route to tunability in colloidal gel rheology.

SUPPLEMENTARY MATERIAL

See the [supplementary material](#) for the following: *Videos S1–S2*: Filled gels (S1: $\phi_f = 0.1$; S2: $\phi_f = 0.4$) under creep test. Within the slice of thickness = $10d_g$ in the flow-gradient plane, only interacting pairs are shown as interparticle bonds,

where the color and width represent pair type and force magnitude, respectively. The time step (shown at the top-left corner) interval between frames is logarithmically scaled. *Videos S3–S4*: Filled gels (S3: $\phi_f = 0.1$; S4: $\phi_f = 0.4$) under creeping with SPP (measured at rest) highlighted in red. For better visualization, colloids and fillers are set to be translucent. *Experiments*: The absence of colloidal “halos” around hydrophobic fillers precludes strong gel–filler attractions; Rheology of a $\phi_g = 0.1$ colloidal gel justifies our measurement protocol. *Simulations*: Demonstration of modulus decomposition; dynamic tests of a $\phi_g = 0.1$ colloidal gel; structure factors of colloidal gels; yield stress upon filler removal as a function of $\phi_f(1 - \alpha)$; elastic modulus upon filler removal; shortest percolation path (SPP) in colloidal gels; gel–gel structure factor with small fillers ($d_f = d_g$).

ACKNOWLEDGMENTS

We thank John Royer and Wilson Poon for experimental assistance and George Petekidis and Tiancong Zhao for fruitful discussions. This work was supported by the National Natural Science Foundation of China (Nos. 12404235, 12174390, and 12150610463) and Wenzhou Institute, University of Chinese Academy of Sciences (No. WIUCASQD2020002). C.N. acknowledges support from the Royal Academy of Engineering under the Research Fellowship scheme and from the Leverhulme Trust under Research Project Grant No. RPG-2022-095.

AUTHOR DECLARATIONS

Conflict of Interest

The authors have no conflicts to disclose.

DATA AVAILABILITY

The data that support the findings of this study are available from the corresponding author upon reasonable request.

REFERENCES

- Royall, C. P., M. A. Faers, S. L. Fussell, and J. E. Hallett, “Real space analysis of colloidal gels: Triumphs, challenges and future directions,” *J. Phys.: Condens. Matter* **33**, 453002 (2021).
- Bonn, D., M. M. Denn, L. Berthier, T. Divoux, and S. Manneville, “Yield stress materials in soft condensed matter,” *Rev. Mod. Phys.* **89**, 035005 (2017).
- Sprakler, J., S. B. Lindström, T. E. Kodger, and D. A. Weitz, “Stress enhancement in the delayed yielding of colloidal gels,” *Phys. Rev. Lett.* **106**, 248303 (2011).
- Bantawa, M., B. Keshavarz, M. Geri, M. Bouzid, T. Divoux, G. H. McKinley, and E. Del Gado, “The hidden hierarchical nature of soft particulate gels,” *Nat. Phys.* **19**, 1178–1184 (2023).
- Keshavarz, B., D. G. Rodrigues, J.-B. Champenois, M. G. Frith, J. Ilavsky, M. Geri, T. Divoux, G. H. McKinley, and A. Poulesquer, “Time-connectivity superposition and the gel/glass duality of weak colloidal gels,” *Proc. Natl. Acad. Sci. U.S.A.* **118**, e2022339118 (2021).
- Rose, S., A. Prevoteau, P. Elzière, D. Hourdet, A. Marcellan, and L. Leibler, “Nanoparticle solutions as adhesives for gels and biological tissues,” *Nature* **505**, 382–385 (2014).

- [7] Ubbink, J., “Soft matter approaches to structured foods: From ‘cook-and-look’ to rational food design?,” *Faraday Discuss.* **158**, 9–35 (2012).
- [8] E. Del Gado, D. Fiocco, G. Foffi, S. Manley, V. Trappe, and A. Zacccone, “Colloidal gelation,” in *Fluids, Colloids and Soft Materials* (John Wiley & Sons, Ltd, New York, 2016), Chap. 14, pp. 279–291.
- [9] Manley, S., H. M. Wyss, K. Miyazaki, J. C. Conrad, V. Trappe, L. J. Kaufman, D. R. Reichman, and D. A. Weitz, “Glasslike arrest in spinodal decomposition as a route to colloidal gelation,” *Phys. Rev. Lett.* **95**, 238302 (2005).
- [10] Patrick Royall, C., S. R. Williams, T. Ohtsuka, and H. Tanaka, “Direct observation of a local structural mechanism for dynamic arrest,” *Nat. Mater.* **7**, 556–561 (2008).
- [11] Hsiao, L. C., R. S. Newman, S. C. Glotzer, and M. J. Solomon, “Role of isostaticity and load-bearing microstructure in the elasticity of yielded colloidal gels,” *Proc. Natl. Acad. Sci. U.S.A.* **109**, 16029–16034 (2012).
- [12] Wang, Y., M. Tateno, and H. Tanaka, “Distinct elastic properties and their origins in glasses and gels,” *Nat. Phys.* **20**, 1171–1179 (2024).
- [13] Lu, P. J., E. Zaccarelli, F. Ciulla, A. B. Schofield, F. Sciortino, and D. A. Weitz, “Gelation of particles with short-range attraction,” *Nature* **453**, 499–503 (2008).
- [14] Koumakis, N., E. Moghimi, R. Besseling, W. C. K. Poon, J. F. Brady, and G. Petekidis, “Tuning colloidal gels by shear,” *Soft Matter* **11**, 4640–4648 (2015).
- [15] Gibaud, T., N. Dagès, P. Lidon, G. Jung, L. C. Ahouré, M. Sztucki, A. Poulesquen, N. Hengl, F. Pignon, and S. Manneville, “Rheoacoustic gels: Tuning mechanical and flow properties of colloidal gels with ultrasonic vibrations,” *Phys. Rev. X* **10**, 011028 (2020).
- [16] Wei, M., M. Y. Ben Zion, and O. Dauchot, “Reconfiguration, interrupted aging, and enhanced dynamics of a colloidal gel using photo-switchable active doping,” *Phys. Rev. Lett.* **131**, 018301 (2023).
- [17] Omar, A. K., Y. Wu, Z.-G. Wang, and J. F. Brady, “Swimming to stability: Structural and dynamical control via active doping,” *ACS Nano* **13**, 560–572 (2019).
- [18] Muhammed Shameem, M., S. Sasikanth, R. Annamalai, and R. Ganapathi Ramam, “A brief review on polymer nanocomposites and its applications,” *Mater. Today: Proc.* **45**, 2536–2539 (2021).
- [19] Spanoudakis, J., and R. J. Young, “Crack propagation in a glass particle-filled epoxy resin,” *J. Mater. Sci.* **19**, 473–486 (1984).
- [20] Moosberg-Bustnes, H., B. Lagerblad, and E. Forssberg, “The function of fillers in concrete,” *Mater. Struct.* **37**, 74–81 (2004).
- [21] Ganesan, V., and A. Jayaraman, “Theory and simulation studies of effective interactions, phase behavior and morphology in polymer nanocomposites,” *Soft Matter* **10**, 13–38 (2014).
- [22] Mahaut, F., X. Chateau, P. Coussot, and G. Ovarlez, “Yield stress and elastic modulus of suspensions of noncolloidal particles in yield stress fluids,” *J. Rheol.* **52**, 287–313 (2008).
- [23] Jiang, Y., S. Makino, J. R. Royer, and W. C. K. Poon, “Flow-switched bistability in a colloidal gel with non-Brownian grains,” *Phys. Rev. Lett.* **128**, 248002 (2022).
- [24] Li, Y., J. R. Royer, J. Sun, and C. Ness, “Impact of granular inclusions on the phase behavior of colloidal gels,” *Soft Matter* **19**, 1342–1347 (2023).
- [25] Jiang, Y., and R. Seto, “Colloidal gelation with non-sticky particles,” *Nat. Commun.* **14**(1), 2773 (2023).
- [26] Ferreiro-Córdova, C., G. Foffi, O. Pitois, C. Guidolin, M. Schneider, and A. Salonen, “Stiffening colloidal gels by solid inclusions,” *Soft Matter* **18**, 2842–2850 (2022).
- [27] Jia, D., H. Cheng, and C. C. Han, “Interplay between caging and bonding in binary concentrated colloidal suspensions,” *Langmuir* **34**, 3021–3029 (2018).
- [28] Jia, D., J. V. Hollingsworth, Z. Zhou, H. Cheng, and C. C. Han, “Coupling of gelation and glass transition in a biphasic colloidal mixture—From gel-to-defective gel-to-glass,” *Soft Matter* **11**, 8818–8826 (2015).
- [29] Duduta, M., B. Ho, V. C. Wood, P. Limthongkul, V. E. Brunini, W. C. Carter, and Y.-M. Chiang, “Semi-solid lithium rechargeable flow battery,” *Adv. Energy Mater.* **1**, 511–516 (2011).
- [30] Mohraz, A., E. R. Weeks, and J. A. Lewis, “Structure and dynamics of biphasic colloidal mixtures,” *Phys. Rev. E* **77**, 060403 (2008).
- [31] Dellatolas, I., M. Bantawa, B. Damerau, M. Guo, T. Divoux, E. Del Gado, and I. Bischofberger, “Local mechanism governs global reinforcement of nanofiller-hydrogel composites,” *ACS Nano* **17**, 20939–20948 (2023).
- [32] Das, D., T. Kar, and P. K. Das, “Gel-nanocomposites: Materials with promising applications,” *Soft Matter* **8**, 2348–2365 (2012).
- [33] Park, J. H., S. H. Sung, S. Kim, and K. H. Ahn, “Significant agglomeration of conductive materials and the dispersion state change of the Ni-rich NMC-based cathode slurry during storage,” *Ind. Eng. Chem. Res.* **61**, 2100–2109 (2022).
- [34] Larsen, T., J. R. Royer, F. H. J. Laidlaw, W. C. K. Poon, T. Larsen, S. J. Andreasen, and J. D. C. Christiansen, “Controlling the rheoelectric properties of graphite/carbon black suspensions by ‘flow switching’,” *Rheol. Acta* **63**, 283–289 (2024).
- [35] Pradeep, S., P. E. Arratia, and D. J. Jerolmack, “Origins of complexity in the rheology of soft earth suspensions,” *arXiv:2312.15092 [cond-mat.soft]* (2023).
- [36] Suratwala, T., M. Hanna, E. Miller, P. Whitman, I. Thomas, P. Ehrmann, R. Maxwell, and A. Burnham, “Surface chemistry and trimethylsilyl functionalization of Stöber silica sols,” *J. Non-Cryst. Solids* **316**, 349–363 (2003).
- [37] Thompson, A. P., H. M. Aktulgä, R. Berger, D. S. Bolintineanu, W. M. Brown, P. S. Crozier, P. J. in’t Veld, A. Kohlmeyer, S. G. Moore, T. D. Nguyen, R. Shan, M. J. Stevens, J. Tranchida, C. Trott, and S. J. Plimpton, “LAMMPS—A flexible simulation tool for particle-based materials modeling at the atomic, meso, and continuum scales,” *Comput. Phys. Commun.* **271**, 108171 (2022).
- [38] Though still weaker than the hydrophobic attraction in experiments ($\gtrsim 10^2 k_B T$), we confirm that such a value causes irreversible bonding and is sufficient to produce a fractal gel network, similar to that resulting from stronger attraction.
- [39] Viehman, D. C., and K. S. Schweizer, “Theory of gelation, vitrification, and activated barrier hopping in mixtures of hard and sticky spheres,” *J. Chem. Phys.* **128**, 084509 (2008).
- [40] Eberle, A. P. R., R. Castañeda-Priego, J. M. Kim, and N. J. Wagner, “Dynamical arrest, percolation, gelation, and glass formation in model nanoparticle dispersions with thermoreversible adhesive interactions,” *Langmuir* **28**, 1866–1878 (2012).
- [41] Colombo, J., and E. Del Gado, “Stress localization, stiffening, and yielding in a model colloidal gel,” *J. Rheol.* **58**, 1089–1116 (2014).
- [42] Stukowski, A., “Visualization and analysis of atomistic simulation data with OVITO—The open visualization tool,” *Model. Simul. Mater. Sci. Eng.* **18**, 015012 (2009).
- [43] Differing from conventional creep test, we do not equilibrate the sample (by either replacing with a fresh sample or applying the rejuvenation-recovery protocol) between each imposed stress-step, because of the limited amount of samples and aging effects.
- [44] Cabriolu, R., J. Horbach, P. Chaudhuri, and K. Martens, “Precursors of fluidisation in the creep response of a soft glass,” *Soft Matter* **15**, 415–423 (2019).
- [45] Shih, W.-H., W. Y. Shih, S.-I. Kim, J. Liu, and I. A. Aksay, “Scaling behavior of the elastic properties of colloidal gels,” *Phys. Rev. A* **42**, 4772–4779 (1990).

07 January 2025 08:51:26

- [46] Kao, P.-K., M. J. Solomon, and M. Ganesan, "Microstructure and elasticity of dilute gels of colloidal discoids," *Soft Matter* **18**, 1350–1363 (2022).
- [47] Petekidis, G., and N. J. Wagner, "Rheology of colloidal glasses and gels," in *Theory and Applications of Colloidal Suspension Rheology*, Cambridge Series in Chemical Engineering, edited by N. J. Wagner and J. Mewis (Cambridge University, Cambridge, 2021), pp. 173–226.
- [48] Barwick, S., and M. E. Möbius, "The elastic response of graphene oxide gels as a crumpling phenomenon," *Soft Matter* **18**, 8223–8228 (2022).
- [49] Roy, S., and M. S. Tirumkudulu, "Micro-mechanical theory of shear yield stress for strongly flocculated colloidal gel," *Soft Matter* **16**, 1801–1809 (2020).
- [50] Meyer, E. E., K. J. Rosenberg, and J. Israelachvili, "Recent progress in understanding hydrophobic interactions," *Proc. Natl. Acad. Sci. U.S.A.* **103**, 15739–15746 (2006).
- [51] Santos, A. P., D. S. Bolintineanu, G. S. Grest, J. B. Lechman, S. J. Plimpton, I. Srivastava, and L. E. Silbert, "Granular packings with sliding, rolling, and twisting friction," *Phys. Rev. E* **102**, 032903 (2020).
- [52] Guazzelli, É., and O. Pouliquen, "Rheology of dense granular suspensions," *J. Fluid Mech.* **852**, P1 (2018).
- [53] Gravelle, A. J., and A. G. Marangoni, "A new fractal structural-mechanical theory of particle-filled colloidal networks with heterogeneous stress translation," *J. Colloid Interface Sci.* **598**, 56–68 (2021).
- [54] Zhang, S., E. Stanifer, V. V. Vasisht, L. Zhang, E. Del Gado, and X. Mao, "Prestressed elasticity of amorphous solids," *Phys. Rev. Res.* **4**, 043181 (2022).
- [55] Sorichetti, V., V. Hugouvieux, and W. Kob, "Structure and dynamics of a polymer-nanoparticle composite: Effect of nanoparticle size and volume fraction," *Macromolecules* **51**, 5375–5391 (2018).
- [56] Tsurusawa, H., S. Arai, and H. Tanaka, "A unique route of colloidal phase separation yields stress-free gels," *Sci. Adv.* **6**, eabb8107 (2020).
- [57] Zhang, H., W. You, F. Bian, and W. Yu, "Heterogeneous percolation in poly(methylvinylsiloxane)/silica nanocomposites: The role of polymer–particle interaction," *Macromolecules* **55**, 8834–8845 (2022).
- [58] The quantitative difference may result from the difference in interaction range and contact mechanics.
- [59] Tian, B., X. Liu, C. Yu, F. Gao, Q. Luo, S. Xie, B. Tu, and D. Zhao, "Microwave assisted template removal of siliceous porous materials," *Chem. Commun.* (11), 1186–1187 (2002).
- [60] Poon, W., and M. Haw, "Mesoscopic structure formation in colloidal aggregation and gelation," *Adv. Colloid Interface Sci.* **73**, 71–126 (1997).
- [61] van Doorn, J. M., J. E. Verweij, J. Sprakel, and J. van der Gucht, "Strand plasticity governs fatigue in colloidal gels," *Phys. Rev. Lett.* **120**, 208005 (2018).
- [62] Nabizadeh, M., F. Nasirian, X. Li, Y. Saraswat, R. Waheibi, L. C. Hsiao, D. Bi, B. Ravandi, and S. Jamali, "Network physics of attractive colloidal gels: Resilience, rigidity, and phase diagram," *Proc. Natl. Acad. Sci. U.S.A.* **121**, e2316394121 (2024).
- [63] Dokholyan, N. V., Y. Lee, S. V. Buldyrev, S. Havlin, P. R. King, and H. E. Stanley, "Scaling of the distribution of shortest paths in percolation," *J. Stat. Phys.* **93**, 603–613 (1998).
- [64] Tsurusawa, H., and H. Tanaka, "Hierarchical amorphous ordering in colloidal gelation," *Nat. Phys.* **19**, 1171–1177 (2023).
- [65] Keene, M. T. J., R. Denoyel, and P. L. Llewellyn, "Ozone treatment for the removal of surfactant to form mcm-41 type materials," *Chem. Commun.* (20), 2203–2204 (1998).
- [66] Ghaedi, H., and M. Zhao, "Review on template removal techniques for synthesis of mesoporous silica materials," *Energy Fuels* **36**, 2424–2446 (2022).
- [67] Zhang, X.-Z., D.-Q. Wu, and C.-C. Chu, "Synthesis, characterization and controlled drug release of thermosensitive IPN–PNIPAAm hydrogels," *Biomaterials* **25**, 3793–3805 (2004).
- [68] Xie, M., Y. Sun, J. Wang, Z. Fu, L. Pan, Z. Chen, J. Fu, and Y. He, "Thermo-sensitive sacrificial microsphere-based bioink for centimeter-scale tissue with angiogenesis," *Int. J. Bioprint* **8**(4), 599 (2022).
- [69] Farjami, T., and A. Madadlou, "An overview on preparation of emulsion-filled gels and emulsion particulate gels," *Trends Food Sci. Technol.* **86**, 85–94 (2019).
- [70] Gravelle, A. J., and A. G. Marangoni, "Effect of matrix architecture on the elastic behavior of an emulsion-filled polymer gel," *Food Hydrocoll.* **119**, 106875 (2021).
- [71] Torre, K. W., and J. de Graaf, "Structuring colloidal gels via micro-bubble oscillations," *Soft Matter* **19**, 2771–2779 (2023).
- [72] Saint-Michel, B., G. Petekidis, and V. Garbin, "Tuning local microstructure of colloidal gels by ultrasound-activated deformable inclusions," *Soft Matter* **18**, 2092–2103 (2022).
- [73] Müller, F. J., L. Isa, and J. Vermant, "Toughening colloidal gels using rough building blocks," *Nat. Commun.* **14**(1), 5309 (2023).

07 January 2025 15:129